



## THE EFFECT OF SINGLE AND DOUBLE-DOPED ADDITION ON 8YSZ COATING LAYERS DEPOSITED ON INCONEL 625 BY ELECTROPHORETIC DEPOSITION

Kurotun Aini<sup>1,2,\*</sup>, Fina Fitratan Amaliyah<sup>1</sup>, Eni Sugiarti<sup>2</sup>, Resetiana Dwi Desiati<sup>2</sup>, Nurul Latifah<sup>2</sup>, Safitry Ramandhany<sup>2</sup>, Ihah Fadilah<sup>2</sup>, Aunillah Putri El Nasihah<sup>2</sup>

<sup>1</sup>Department of Physics, State Islamic University Sultan Maulana Hasanuddin Banten  
Jl. Syech Nawawi Al-Bantani, Serang, Banten, Indonesia 42171

<sup>2</sup>Research Center for Advanced Materials, National Research and Innovation Agency  
B.J. Habibie Sains and Technology Area, Banten, Indonesia 15314

\*Email: kurotunaini44@gmail.com

Received: 31-1-2025, Revised: 18-06-2025, Accepted: 20-06-2025

### Abstract

The ceramic layers of 8 mol% yttria-stabilized zirconia (8YSZ), singly doped with  $Fe_2O_3$  and doubly doped with  $Fe_2O_3$  and  $Al_2O_3$ , have been deposited successfully on Inconel 625 substrates by the EPD (electrophoretic deposition) process. The oxide doping influenced the stability of the EPD suspension and affected the density of the resultant layer. In order to improve the adhesion between the layer and the substrate, a two-step sintering was performed up to 1200 °C for a total duration of 4 hours in a horizontal vacuum furnace, with a heating rate of 2 °C per minute in an Argon gas atmosphere. FE-SEM (field emission scanning electron microscopy) and vickers hardness tests were employed to investigate the effect of single and double doping on the morphology and hardness of the coating layers, respectively. EDS (energy dispersive spectroscopy) was employed to analyze the elemental composition of the layers, while XRD (x-ray diffractometry) was utilized to determine the crystalline phases. The results indicated that the double-doped coating sample possesses a better microstructure and the layer with double doping exhibits a denser microstructure and reduced porosity (3.84%) in contrast to the single doping layer (6.05%). The vickers hardness test indicates a rise in hardness from 65.3 HV with single doping to 283.78 HV with double-doping layers, due to the presence of  $Al_2O_3$  as the interstitial agent, which reduces the layer's porosity and enhances adhesion between the layer and the substrate. Furthermore, the addition of  $Al_2O_3$  as the double dopant may impede the  $t \rightarrow m$  phase transformation, leading to enhanced thermal stability in the double-doped coating sample compared to the single-doped coating sample. This study shows that double doping techniques can improve the efficiency of ceramic coatings for high-temperature applications, such as gas turbine components, and also giving opportunities for more research in oxidation, corrosion, and erosion testing.

**Keywords:**  $Al_2O_3$ , electrophoretic deposition,  $Fe_2O_3$ , inconel 625, yttrium-stabilized zirconia

### 1. INTRODUCTION

Nickel-based superalloys, such as Inconel 625, are commonly used for parts that function at high temperatures, including gas turbine blades and aircraft vanes, due to their remarkable mechanical properties at high temperatures [1]. Nevertheless, prolonged exposure to such high temperatures frequently results in degradation caused by the passage of hot combustion gases

that oxidize the components. Consequently, TBC (thermal barrier coatings) are often used as an insulation layer on nickel-based hot parts to enhance the component lifetime and improve efficiency [1]-[7].

The ceramic-based top layer in the TBC system has continual improvements regarding materials and coating techniques. The top layer typically consists of yttria-partially stabilized

DOI: 10.55981/metalurgi.2024.770

© 2024 Author(s). This is an open access article under the CC BY-SA license (<http://creativecommons.org/licenses/by-sa/4.0>)

Metalurgi is Sinta 2 Journal (<https://sinta.kemdikbud.go.id/journals/profile/3708>) accredited by Ministry of Education, Culture, Research, and Technology, Republic Indonesia

zirconia, due to its exceptional characteristics, including low thermal conductivity and a high thermal expansion coefficient, which are nearly acceptable with superalloys [2]. Ytria-stabilized zirconia (YSZ) is commonly used as the topmost layer by techniques such as EB-PVD (electron beam physical vapor deposition), APS (air plasma spraying), or CVD (chemical vapor deposition) [3].

Established methods have been widely employed for the creation of YSZ layers. Nonetheless, the intricacy of the required equipment, production expenses, and restricted adaptability have emerged as concerns [4]. Other studies have taken efforts to create a simple, flexible, and cost-effective coating technique [7]. This process is known as EPD (electrophoretic deposition). The EPD technique is a cost-effective and straightforward alternative to create simple, versatile, and economical coatings. This technique facilitates the uniform deposition of charged ceramic particles from a liquid suspension onto the surface of a conductive substrate via an electric field [5]-[6].

The suspension stability, electric source, and deposition duration are parameters that may affect the characteristics of the layer deposited with the EPD method [9]-[10]. The ideal coating suspension must be metastable, allowing dissolved particles to adhere to the substrate without excessive sedimentation in the bath [9]. The rate of deposition increases as voltage rises. Nonetheless, the use of high voltage may create a substantial electric field, which could compromise the coating quality beyond a certain threshold. High-voltage application can lead to the rapid deposition of ceramic particles onto the substrate. This may impact deposition quality and result in layers with uneven structures, leading to porosity and the formation of cracks [10]. Consequently, an optimal voltage application is necessary for the deposition of ceramic particles, which, according to the literature, occurs at a voltage below 100 V [9]. In addition, the duration of deposition affects the thickness of the YSZ layer produced by EPD. Bai et al., [7] revealed that the ideal duration for the EPD process utilizes a voltage gradient of 3 to 15 minutes, during which the voltage gradient method for coating typically results in a YSZ layer thickness of 300-400  $\mu\text{m}$ .

The freshly coated YSZ ceramic layer requires sintering to promote recrystallization, increase layer density, and enhance adhesion between the layer and substrate [3]. The temperature necessary for the YSZ densification must exceed 1300 °C, due to the high melting

point of YSZ [11]. Schulz et al. performed sintering on YSZ layers at temperatures ranging from 1200 to 1400 °C [12]. The results indicated that during single-stage sintering, a combination of tetragonal (t) and cubic (c) phases, as well as several monoclinic (m) phases, were formed. The existence of the m-phase after sintering at 1400 °C is detrimental due to its potential to induce thermal stress. The stress induced by cooling during the t→m phase transformation will impact the durability of the coating system [12]. Consequently, additional elements or oxide doping are required to control the t→m phase transformation and maintain the capacity to reduce the sintering temperature.

The investigation of various additives, such as CoO, CuO, Fe<sub>2</sub>O<sub>3</sub>, Bi<sub>2</sub>O<sub>3</sub>, SiO<sub>2</sub>, Al/Al<sub>2</sub>O<sub>3</sub>, ZrN, Sc<sub>2</sub>O<sub>3</sub>, and Ni/NiO, has been conducted to lower the sintering temperature of the YSZ layer [9], [14]-[15]. Kalinina et al. indicated that the addition of Al<sub>2</sub>O<sub>3</sub> into the YSZ suspension during deposition by the EPD method produced a dense and uniform layer with minimal porosity after sintering at 1200 °C [14]. In addition, Bai et al., [7] demonstrated that Fe<sub>2</sub>O<sub>3</sub> serves as a proficient sintering aid, lowering the sintering temperature of refractory ceramics and enhancing the densification of tetravalent oxides, including ZrO<sub>2</sub>. Consequently, it can be inferred that employing Al<sub>2</sub>O<sub>3</sub> and Fe<sub>2</sub>O<sub>3</sub> as individual oxide dopants may improve the microstructure of the YSZ layer by distinct enhancement processes.

Guo et al., [15] investigated the YSZ coatings with Fe<sub>2</sub>O<sub>3</sub> as a single dopant. Their findings demonstrated that the addition of Fe<sub>2</sub>O<sub>3</sub> doping into the 3YSZ layer enhances the grain size; nevertheless, the enhancement is insignificant, resulting in a less dense layer structure, with ceramic phase instability perhaps serving as a contributing factor. In contrast, the use of double or multiple doping on the ZrO<sub>2</sub> coating is recognized to produce a ZrO<sub>2</sub> ceramic layer with remarkable phase stability. The addition of Al<sub>2</sub>O<sub>3</sub>, CeO<sub>2</sub>, Yb<sub>2</sub>O<sub>3</sub>, and Gd<sub>2</sub>O<sub>3</sub> via the APS method on ZrO<sub>2</sub> coating is recognized to substantially reduce phase transition, enhance thermal stability, and improve bond strength [16]. Consequently, it can be inferred that double oxide doping possesses significant potential as a sintering agent that enhances the microstructure of the YSZ layer.

The use of double oxide doping on YSZ layers via the EPD method is recognized as constrained and under-researched. This study aims to investigate the impact of single (Fe<sub>2</sub>O<sub>3</sub>) and double (Fe<sub>2</sub>O<sub>3</sub>+Al<sub>2</sub>O<sub>3</sub>) oxide doping on 8YSZ layers in relation to microstructure, layer

porosity, surface hardness, phase formation, and phase stability to evaluate its efficacy as a protective layer for Inconel 625 substrates. In addition, the flow behavior of various 8YSZ suspensions using the EPD method was observed to comprehend the properties of the 8YSZ suspension affected by oxide doping. Consequently, a comprehensive examination of the impact of oxide doping on the development of the 8YSZ layer may be conducted.

## 2. MATERIALS AND METHODS

### 2.1 Sample Preparation

The present study utilized Inconel 625 (Nilaco, Japan) with dimensions of 15 x 15 x 1 mm as a substrate. With the chemical composition of Inconel 625 in wt.% such as: (20-23)Cr, (8-10)Mo, 5Fe, (3.15-4.15)Nb+Ta, 1Co, 0.5Mn, 0.5Si, 0.4Al, 0.4Ti, 0.1C, 0.015P, 0.015 S, with Ni as the balance. The substrate was polished in succession with SiC paper of grit sizes 100, 500, and 800. The substrate was ultrasonically cleaned in acetone for 180 seconds following polishing.

Table 1. Mass percentage composition of the analyzed suspension (wt.%)

Materials	Single-doping suspension	Double-doping suspension
8YSZ	94.52	86.4
Fe <sub>2</sub> O <sub>3</sub>	0.76	0.7
Al <sub>2</sub> O <sub>3</sub>	-	8.6
Iodine	4.73	4.3
Acetyl acetone	50	50
Ethanol	50	50

This study created two types of 8YSZ suspensions for coating via the EPD procedure to investigate the impact of the oxide doping addition method: single-doping suspension and double-doping suspension, as detailed in Table 1. The suspension was prepared by mixing the commercial 8YSZ powder (8 mol% Y<sub>2</sub>O<sub>3</sub>, >99%, Kanto, Japan), Iron (III) Oxide (0.02 mol% Fe<sub>2</sub>O<sub>3</sub>, >99%, technical powder), Aluminum Oxide (Al<sub>2</sub>O<sub>3</sub> powder, Kanto Chemical Co., Inc.), and iodine as a dispersant in a solvent. Acetyl acetone (ACAC, >99%, Merck) and ethanol (Et>99%, Merck) were utilized as the solvent in a 1:1 volume ratio. A viscosity test was conducted using the ViscoQC100 rotational viscometer on days 1, 2, 3, 4, and 8 to evaluate the stability and adequacy of the suspension for the deposition process. This test evaluates the flow properties of fluid viscosity and assesses the

stability of the suspension for the deposition process using EPD.

### 2.2 EPD Procedure

Before the implementation of EPD, the suspension was mixed using a magnetic stirrer followed by sonication for 5 minutes. This study employed a cathodic EPD process using a nickel plate as the anode and Inconel 625 as the cathode, with a distance of approximately 3 cm between the anode and cathode, as illustrated in Figure 1(a).

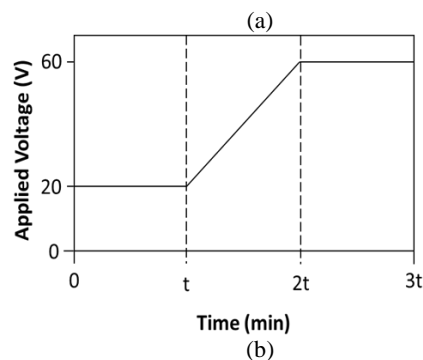
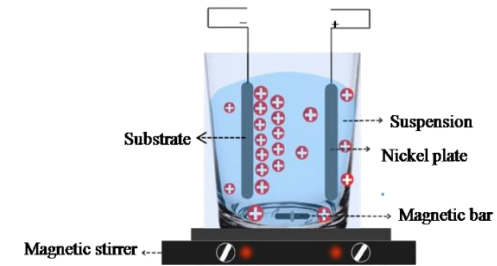


Figure 1. Schematic representation of (a) the EPD process and (b) the applied voltage

The DC power supply (XANTREX, XHR 60-18) was used as the voltage source for the EPD process. The voltage treatment was conducted using a two-stage parameter, consisting of a constant voltage (20 V), a gradient voltage (20-60 V), and a final constant voltage (60 V), with a total duration of 12 minutes, as depicted in Fig. 1(b).

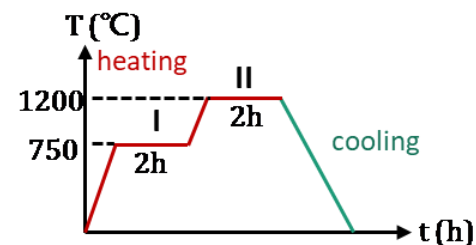


Figure 2. Schematic of the sintering profile

The freshly coated sample was dried at room temperature for 24 hours and then sintered in a horizontal vacuum furnace with a heating rate of 2 °C per minute in an Argon atmosphere.

Sintering was performed in two stages: the initial stage at 750 °C for 2 hours, followed by a second stage at 1200 °C for 2 hours. Figure 2 illustrates the schematic representation of the two-stage sintering profile.

### 2.3 Characterization

The coating samples were analyzed using field emission-scanning electron microscopy (FE-SEM, JEOL, JIB4610F) combined with EDS (energy dispersive spectroscopy), Oxford, X-Max 50 mm<sup>2</sup> to study the elemental composition and examine the surface and cross-sectional microstructure. Analysis of cross-sectional images using ImageJ software was conducted to evaluate the porosity of the layer. The XRD (x-ray diffraction) SmartLab, Rigaku employs Cu K $\alpha$  radiation (wavelength, 1.5405 Å), operating at 40 kV and 30 mA, with a 2 $\theta$  range of 10° to 90° to identify the phases present in the coating. Subsequently, to assess the mechanical properties of the coating, the surface hardness of the coating samples was evaluated utilizing a hardness tester (Mitech, MH600).

## 3. RESULTS AND DISCUSSION

### 3.1 Viscosity of the YSZ Suspension

In the EPD process, particles will migrate towards the liquid phase upon the application of an electric field. Consequently, several suspension parameters need to be considered throughout the coating process utilizing the EPD method, including a high dielectric constant, low conductivity, and low viscosity. The viscosity of the suspension was observed on the first, second, third, fourth, and eighth days to analyze the progression of viscosity and the flow characteristics of the suspension over time[9]. The viscosity on the eighth day demonstrates optimal stability according to the daily viscosity measurements.

Figure 3 shows that the viscosity of the 8YSZ double-doping suspension is notably higher than that of the single-doping suspension, with values ranging from 0.928 to 1.031 m.Pa.s for single doping and from 0.979 to 1.288 m.Pa.s for double doping. Both suspensions have low viscosity values and comparable flow behavior curves, specifically demonstrating shear-thinning characteristics. Upon closer examination, the flow behavior curve of the double-doping suspension appears to be more unstable than that of the single-doping suspension. This is beneficial because, if the suspension is excessively stable, the repulsive forces among the particles will not be overcome by the electric field, hence inhibiting deposition. Some models

for EPD indicate that the suspension should be unstable in proximity to the electrodes [9].

The instability of the double-doping suspension can be attributed to the presence of Al<sub>2</sub>O<sub>3</sub>. Al<sub>2</sub>O<sub>3</sub> is an acidic oxide that can absorb free oxygen ions, leading to a tetrahedral structure of four-coordinate aluminum oxide, which enhances viscosity and creates a well-dispersed solution [18]. Therefore, it can be concluded that the double-doping suspension exhibits ideal conditions for deposition using the EPD method, with a viscosity value of 1.09 mPa.s as the reference [8].

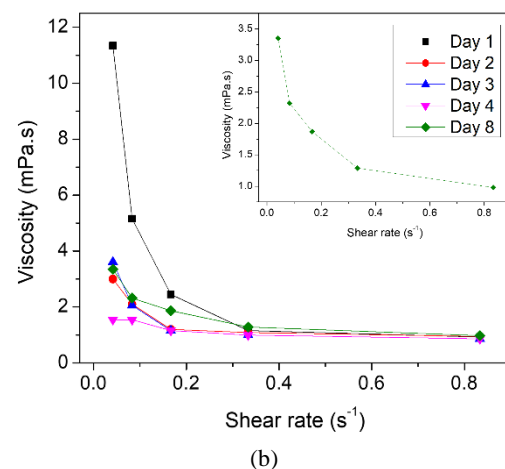
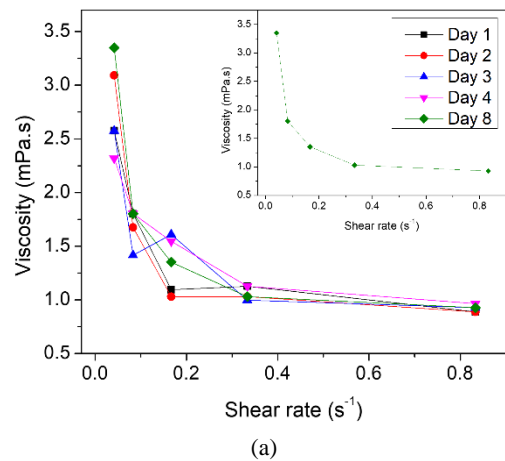


Figure 3. Correlation between shear rate and viscosity of 8YSZ suspension: (a) single-doping, and (b) double-doping

### 3.2 Coating Morphology

Figure 4 shows the cross-sectional image and elemental mapping of the various 8YSZ coating samples influenced by oxide doping. The 8YSZ layer was applied on Inconel 625 via the EPD method and subjected to a two-stage sintering process up to 1200 °C for a total duration of 4 hours. EDS measurements indicated a strong signal of nickel (Ni), chromium (Cr), and molybdenum (Mo), confirming the Inconel 625 substrate composition. In addition, it was observed that the coating layers consisted of two layers: a ceramic layer and an oxide layer. The

ceramic layer consisted of zirconium (Zr), yttrium (Y), and oxygen (O), confirming the YSZ composition, whereas the oxide layer consisted of Cr and O elements, indicating the formation of chromium oxide between the substrate and coating layer.

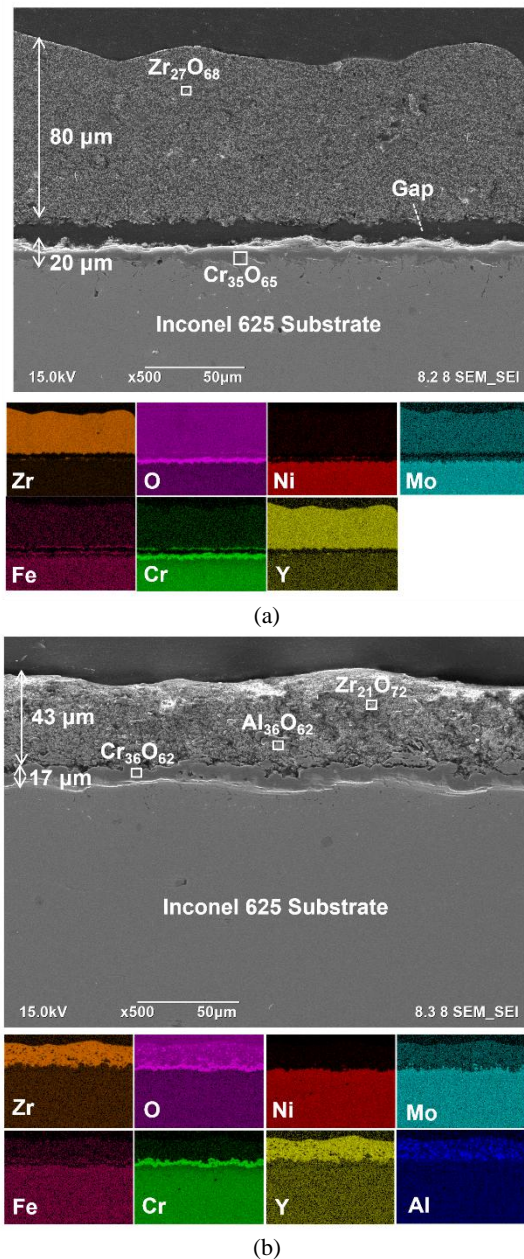


Figure 4. Cross-sectional morphology of the 8YSZ coating samples: (a) single-doping, and (b) double-doping

The coating sample with single doping creates a zirconia layer thickness of approximately 80  $\mu\text{m}$ , whereas the coating sample with double doping results in a thickness of 43  $\mu\text{m}$ . The top coat of zirconia consisted of Zr and O elements with atomic percentages (at%) ranging from 21 to 27 and 68 to 72, respectively. In addition, the oxide layer formed with a thickness of approximately 20  $\mu\text{m}$  for coating samples with single doping and 17  $\mu\text{m}$  for those with double doping. The oxide layer of chromia consisted of

Cr and O elements with atomic percentages (at.%) ranging from 35 to 36 and 62 to 65, respectively. The oxide layer of the two coating samples has been characterized as thermally grown oxide (TGO), with its formation caused by the diffusion of metal ions ( $\text{Cr}^{3+}$ ) from the substrate and the ingress of oxygen ions ( $\text{O}^{2-}$ ) due to elevated temperatures [19].

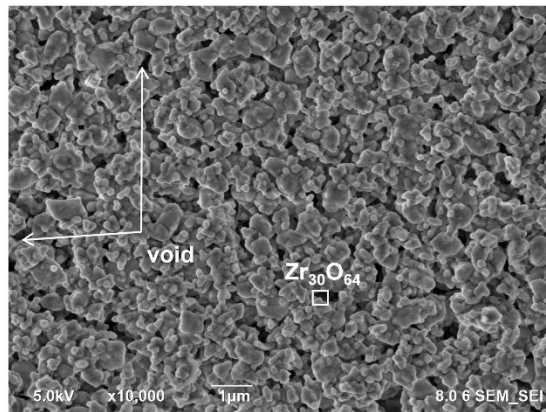
Furthermore, the single-doped coating sample shows a uniform layer with barely visible pores. Nonetheless, there are gaps between the YSZ ceramic layer and the TGO. Defects like pores and gaps in the coating layer may arise due to the volume shrinkage effect of the upper layer during prolonged high-temperature sintering [7]. In contrast, the double-doped coating samples exhibit a dense layer characterized by reduced porosity. This could be attributed to the addition of  $\text{Al}_2\text{O}_3$ , which functions as an interstitial agent that diminishes the layer's porosity. Furthermore,  $\text{Al}_2\text{O}_3$  possesses a high melting point, suggesting it is appropriate as a binding agent for ceramics subjected to high sintering temperatures [20]. The addition of  $\text{Al}_2\text{O}_3$  can reduce the volumetric shrinkage of the coating and improve its adhesion to the metallic substrate. The volumetric expansion from the metal-ceramic reaction partially offsets the sintering shrinkage, facilitating the creation of a ceramic layer with minimal shrinkage [11]. Consequently, the presence of  $\text{Al}_2\text{O}_3$  can improve the adhesion between the layer and the substrate.

### 3.3 Surface Morphology

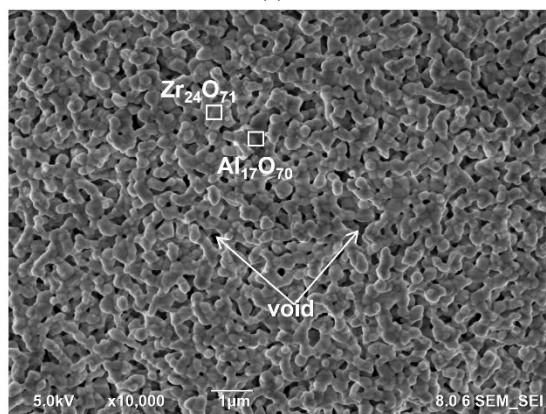
Figure 5 shows the surface morphology of the various 8YSZ coating samples influenced by oxide doping. The surface morphology of the single-doped coating sample exhibits enhanced grain growth, indicated by larger grain sizes than the double-doped coating sample. The high diffusion coefficient of  $\text{Zr}^{4+}$  is primarily responsible for the rapid densification rate of the  $\text{Fe}_2\text{O}_3$  on the 8YSZ layer, due to the interstitial diffusion mechanism of  $\text{Fe}^{3+}$  ions resulting from the simultaneous presence of substitutional and interstitial  $\text{Fe}^{3+}$  ions [15].

Single doping influences the surface morphology of the 8YSZ layer by promoting an increase in grain size. Simultaneously, the surface morphology of the 8YSZ layer with double doping exhibits reduced grain growth. The addition of  $\text{Al}_2\text{O}_3$ , which reinforces the  $\text{ZrO}_2$  ceramic layer interstitially, leads to increased layer hardness and reduced porosity. Kalinina et al., [14] discovered that the addition of  $\text{Al}_2\text{O}_3$  in the EPD suspension during YSZ deposition results in a dense and homogeneous layer with

reduced porosity, therefore,  $\text{Al}_2\text{O}_3$  serves to enhance the hardness of a layer. In addition, vacancies exist in both single-doped and double-doped coating samples. Nevertheless, the single-doped coating samples exhibit larger voids compared to the double-doped coating samples.



(a)



(b)

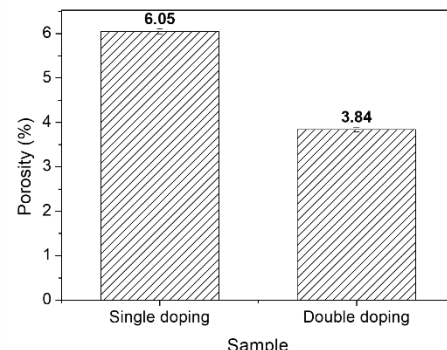
Figure 5. Surface microstructure of the 8YSZ coating sample: (a) single-doping, (b) double-doping

This may relate to the function of  $\text{Al}_2\text{O}_3$  as an interstitial agent in reducing voids. Layers with fewer voids might improve the adherence of the layer. Excessive void content in a coating can diminish the material's strength, as big voids may serve as susceptible areas that facilitate additional damage, including gaps and cracks. Cracks develop in regions with voids resulting from the pressure exerted on the material. Moreover, exposure to high temperatures will result in increased volumetric expansion, potentially leading to the formation of gaps between the coating and the substrate, as illustrated in Fig. 4(a).

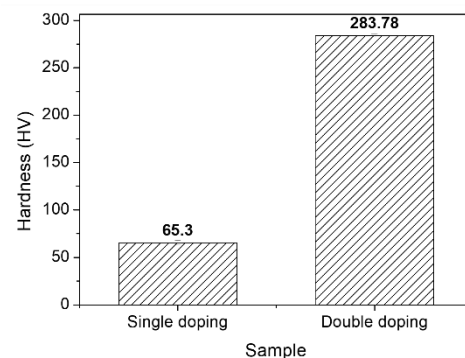
### 3.4 Surface Hardness and Porosity

Figure 6 shows the effect of oxide doping on the surface hardness and porosity of the 8YSZ coating samples. Furthermore, the data about surface hardness and porosity are presented in Table 2.

The results indicate that the double-doped coating sample demonstrates the highest surface hardness of  $283.8 \pm 2.13$  HV and the lowest porosity of  $3.84 \pm 0.05$  %. The increase in surface hardness is due to grain refinement, which reduces porosity during the sintering process.



(a)



(b)

Figure 6. (a) Porosity, and (b) surface hardness of the 8YSZ coating sample

The use of  $\text{Al}_2\text{O}_3$  might improve hardness by acting as a reinforcing phase dispersed throughout the coating layer. The  $\text{Al}_2\text{O}_3$  interstitially enhances the densification of the  $\text{ZrO}_2$  ceramic layer, thus improving the surface hardness.

Table 2. Surface hardness and porosity data of the coating samples

Coating Sample	Porosity (%)	Surface Hardness (HV)
Single-doped	$6.05 \pm 0.06$	$65.3 \pm 2.31$
Double-doped	$3.84 \pm 0.05$	$283.78 \pm 2.13$

The use of double doping on the 8YSZ layer significantly improved surface hardness from 193.8 HV, as reported by Khanali et al., [21].

### 3.5 Phase Analysis

Figure 7 shows the diffraction patterns of the coating samples subjected to single and double doping. Through the reference ICSD (inorganic crystal structure database), the phases formed in

both layers were obtained, namely the tetragonal Zirconia phase (t-ZrO<sub>2</sub>) with reference code (ICSD-98 065-5671) and the monoclinic Zirconia phase (m-ZrO<sub>2</sub>) with reference code (ICSD-98-006-0900).

Analysis of the Rietveld refinement results shows that the crystal size in the single-doping sample is 51.1 nm, while in the double-doping sample it decreases to 30.54 nm. This decrease indicates that the combination of Fe<sub>2</sub>O<sub>3</sub> and Al<sub>2</sub>O<sub>3</sub> dopants is capable of inhibiting crystal growth during the coating process, resulting in a finer and denser microstructure [22]. Additionally, the goodness of fit (GoF) value obtained from the refinement results indicates a better model structure fitting quality to the experimental data in the double-doped samples. The GoF for the single doping sample is 1.67939, while the double doping has a lower GoF of 1.45673, reflecting an improvement in the accuracy of the simulated crystal model. The resulting lattice parameters show significant changes due to variations in doping types, both in the tetragonal and monoclinic phases of ZrO<sub>2</sub>. In the single doping sample, the tetragonal phase lattice parameters were recorded as  $a = b = 3.62877 \text{ \AA}$  and  $c = 5.17936 \text{ \AA}$ , while the monoclinic phase showed  $a = 5.157 \text{ \AA}$ ,  $b = 5.21128 \text{ \AA}$ , and  $c = 5.28903 \text{ \AA}$ . Meanwhile, in the double doping, the tetragonal phase lattice parameters slightly increased along the  $a$  and  $b$  axes to  $3.63423 \text{ \AA}$ , with a decrease along the  $c$  axis to  $5.14794 \text{ \AA}$ . For the monoclinic phase, the lattice parameters shifted to  $a = 5.151 \text{ \AA}$ ,  $b = 5.203 \text{ \AA}$ , and  $c = 5.316 \text{ \AA}$ . The change in lattice parameters indicates that double doping causes a more significant distortion in the crystal structure compared to single doping.

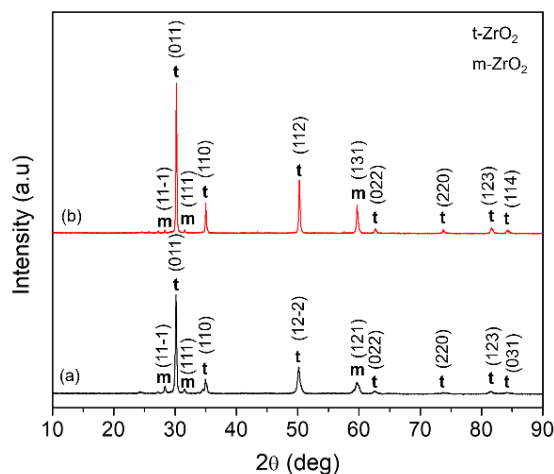


Figure 7. XRD pattern of 8YSZ coating sample: (a) single-doping, and (b) double-doping

The addition of Al<sub>2</sub>O<sub>3</sub> as a double-doped could enhance the prevalence of the tetragonal zirconia phase, as demonstrated in Table 3.

The use of Al<sub>2</sub>O<sub>3</sub> in the double-doped coating sample may improve the stability of the tetragonal zirconia (t-ZrO<sub>2</sub>) phase by being interstitially located in the grain boundaries and impeding the t→m phase transformation. The t-ZrO<sub>2</sub> phase in this coating sample is beneficial due to its superior thermal stability compared to the monoclinic zirconia (m-ZrO<sub>2</sub>) phase.

Table 3. Percentages (%) of monoclinic (m) and tetragonal (t)-ZrO<sub>2</sub> phase

Coating Sample	m-ZrO <sub>2</sub>	t-ZrO <sub>2</sub>
Single-doped	16.1	83.9
Double-doped	3.8	96.2

Consequently, the double-doped coating sample exhibits superior phase stability compared to the single-doped coating sample. A substantial percentage of the m-ZrO<sub>2</sub> phase may compromise the coating due to reduced stability of the zirconia ceramic phase and the formation of micro and macro cracks caused by volumetric expansion. As a result, the coated sample with single doping may demonstrate insufficient resistance to high-pressure and temperature conditions. In contrast, the use of Al<sub>2</sub>O<sub>3</sub> as a double-doped enhances the stability of the t-ZrO<sub>2</sub> by reducing defects, such as cracks or voids, thus protecting the coating and substrate under high-temperature conditions.

#### 4. CONCLUSION

The present study aimed to investigate the microstructure, porosity, surface hardness, and phase formation of the 8YSZ layer with single doping and double doping, generated by the electrophoretic deposition method. The results showed that on the eighth day, the 8YSZ suspension achieved optimal viscosity, particularly in the double-doped suspension, which exhibited a range of 0.979–1.288 mPa.s and demonstrated favorable conditions for EPD due to higher instability. The cross-sectional microstructure of the double-doped coating sample revealed a denser and more compact layer than the single-doped counterpart, which can be attributed to the presence of Al<sub>2</sub>O<sub>3</sub> as an interstitial agent that reduces porosity and enhances adhesion to the substrate. Surface morphology analysis showed reduced grain growth and minimal voids in the double-doped layer, resulting in low porosity ( $3.84 \pm 0.05\%$ ) and high surface hardness ( $283.78 \pm 2.13 \text{ HV}$ ). Furthermore, phase analysis confirmed the

dominance of tetragonal ZrO<sub>2</sub>, with a higher percentage of the t-ZrO<sub>2</sub> phase found in the double-doped sample, likely due to the suppression of the t→m phase transformation by Al<sub>2</sub>O<sub>3</sub> addition, enhancing the thermal stability of the ceramic layer. These findings contribute significantly to the development of cost-effective and efficient thermal barrier coatings for applications such as gas turbine engines. Future work should include cyclic thermal fatigue, oxidation, and erosion testing to evaluate the long-term durability of the coating system under service conditions.

## ACKNOWLEDGMENT

The authors would like to thank the Internal Program of the National Research and Innovation Agency (BRIN) with contract No. B-2/III.10/HK/2025 for financial support of this work.

## REFERENCES

- [1] K. Mondal, L. Nuñez, C. M. Downey, and I. J. Van Rooyen, "Thermal barrier coatings overview: Design, manufacturing, and applications in high-temperature industries," *Ind. Eng. Chem. Res.*, vol. 60, no. 17, pp. 6061-6077, 2021. DOI: 10.1021/acs.iecr.1c00788.
- [2] E. G. Kalinina and E. Y. Pikalova, "Preparation and Properties of Stable Suspensions of ZrO<sub>2</sub>-Y<sub>2</sub>O<sub>3</sub> Powders with Different Particle Sizes for Electrophoretic Deposition," *Inorg. Mater.*, vol. 56, no. 9, pp. 941-948, 2020. DOI: 10.1134/S0020168520090095.
- [3] R. D. Desiati, A. Anawati, and E. Sugiarti, "Two-step sintering improved compaction of electrophoretic-deposited YSZ coatings," *J. Mater. Eng. Perform.*, vol. 31, no. 12, pp. 9888-9899, 2022. DOI: 10.1007/s11665-022-07004-y.
- [4] R. D. Desiati, A. Anawati, and E. Sugiarti, "Microstructural and mechanical characteristics of ceramic composite coating developed by electrophoretic deposition," *IOP Conf. Ser. Mater. Sci. Eng.*, vol. 1098, no. 6, p. 062073, 2021. DOI: 10.1088/1757-899x/1098/6/062073.
- [5] M. J. Zamharir, H. Aghajani, and A. T. Tabrizi, "Evaluation of adhesion strength of TiN layer applied on 316L substrate by electrophoretic deposition," *J. Aust. Ceram. Soc.*, vol. 57, no. 4, pp. 1219-1230, 2021. DOI: 10.1007/s41779-021-00621-1.
- [6] E. G. Kalinina and E. Y. Pikalova, "Electrophoretic deposition of dense anode barrier layers of doped ZrO<sub>2</sub> and BaCeO<sub>3</sub> on a supporting Ce<sub>0.8</sub>Sm<sub>0.2</sub>O<sub>2-δ</sub> solid electrolyte: Problems and search for solutions in SOFC technology," *Int. J. Hydrogen Energy*, vol. 48, no. 59, pp. 22610-22623, 2023. DOI: 10.1016/j.ijhydene.2023.02.042.
- [7] M. Bai, F. Guo, and P. Xiao, "Fabrication of thick YSZ thermal barrier coatings using electrophoretic deposition," *Ceram. Int.*, pp. 1-10, 2014. DOI: 10.1016/j.ceramint.2014.08.021.
- [8] H. Maleki-ghaleh, M. Rekabeslami, M. S. Shakeri, and M. H. Siadati, "Nano-structured yttria-stabilized zirconia coating by electrophoretic deposition," *Appl. Surf. Sci.*, vol. 280, pp. 666-672, 2013. DOI: 10.1016/j.apsusc.2013.04.173.
- [9] L. Besra and M. Liu, "A review on fundamentals and applications of electrophoretic deposition (EPD)," *Prog. Mater. Sci.*, vol. 52, pp. 1-61, 2007. DOI: 10.1016/j.pmatsci.2006.07.001.
- [10] R. D. Desiati, A. Anawati, and E. Sugiarti, "Microstructural and mechanical characteristics of ceramic composite coating developed by electrophoretic deposition," *Mater. Sci. Eng.*, pp. 1-6, 2021. DOI: 10.1088/1757-899X/1098/6/062073.
- [11] Z. Wang, P. Xiao, and J. Shemilt, "Fabrication of composite coatings using a combination of electrochemical methods and reaction bonding process," *J. Eur. Ceram. Soc.*, vol. 20, pp. 1469-1473, 2000. DOI: 10.4236/jbise.2008.13032.
- [12] U. Schulz, "Phase transformation in EB-PVD Yttria partially stabilized Zirconia thermal barrier coatings during annealing," *J. Am. Ceram. Soc.*, vol. 83, no. 4, pp. 904-910, 2000.
- [13] B. Baufeld and O. Van Der Biest, "Lowering the sintering temperature for EPD coatings by applying reaction bonding," *J. Eur. Ceram. Soc.*, vol. 28, pp. 1793-1799, 2008. DOI: 10.1016/j.jeurceramsoc.2007.11.019.
- [14] E. G. Kalinina, A. A. Efimov, and A. P. Safronov, "Preparation of YSZ / Al<sub>2</sub>O<sub>3</sub> composite coatings via electrophoretic deposition of nanopowders," *Inorg. Mater.*, vol. 52, no. 12, pp. 1301-1306, 2016. DOI: 10.1134/S0020168516110054.
- [15] F. Guo and P. Xiao, "Effect of Fe<sub>2</sub>O<sub>3</sub> doping on sintering of yttria-stabilized zirconia," *J. Eur. Ceram. Soc.*, vol. 32, no.

- 16, pp. 4157-4164, 2012. DOI: 10.1016/j.jeurceramsoc.2012.07.035.
- [16] J. Wang, Y. Wang, M. Chen, C. Wang, Y. Yu, Y. Tian, B. Liu, and Q. Jing, "Degradation of CeO<sub>2</sub> and TiO<sub>2</sub> co-stabilized ZrO<sub>2</sub> by the V<sub>2</sub>O<sub>5</sub> molten salts and Na<sub>2</sub>SO<sub>4</sub> + V<sub>2</sub>O<sub>5</sub> molten salts," *Surf. Coatings Technol.*, vol. Volume 437, 2022. DOI: 10.1016/j.surfcoat.2022.128352.
- [17] M. M. De Oliveira, A. A. Couto, G. F. C. Almeida, D. A. P. Reis, N. B. De Lima, and R. Baldan, "Mechanical behavior of inconel 625 at elevated temperatures," *Metals (Basel)*, vol. 9, no. 3, 2019. DOI: 10.3390/met9030301.
- [18] Q. Cheng, Z. Zhang, X. Xing, J. Zheng, and Y. She, "Effect of MgO/Al<sub>2</sub>O<sub>3</sub> on viscosity and thermodynamic properties of high-Titanium slag containing chlorine," *Minerals*, vol. 13, no. 444, pp. 2-13, 2023. DOI:10.3390/min13030444.
- [19] D. R. Clarke and C. G. Levi, "Materials design for the next generation thermal barrier coatings," *Annu. Rev. Mater. Res.*, no. 33, pp. 383-417, 2003. DOI: 10.1146/annurev.matsci.33.011403.113718.
- [20] A. Khezarloo, S. Baghshahi, M. R. Afshar, and A. A. Amadeh, "Sintering and thermal shock behavior of Yttria-stabilized Zirconia coating deposited by electrophoretic method on inconel 738LC superalloy," *Trans. Indian Inst. Met.*, vol. 75, no. 10, pp. 2617-2627, 2022. DOI: 10.1007/s12666-022-02626-1.
- [21] O. Khanali, M. Rajabi, and S. Baghshahi, "Effect of non-aqueous solvents on deposition properties in electrophoretic deposition process of yttria stabilized zirconia nano-powders," *J. Ceram. Process. Res.*, vol. 18, no. 10, pp. 735-742, 2017.
- [22] M. Thakur, A. Vij, F. Singh, and V. S. Rangra, "Spectroscopic studies of metastable tetragonal ZrO<sub>2</sub> nanocrystals," *Spectrochim. Acta - Part A Mol. Biomol. Spectrosc.*, vol. 305, p. 123495, 2024. DOI: 10.1016/j.saa.2023.123495.

